Rational design of bifunctional catalyst based on Mn-containing layered double oxide for the efficient oxidative cleavage of 1,2-diols

Xuan Dai, Pengfei Chen, Xin Wang, Junfeng Qian, Weiyou Zhou*, Mingyang He*

Jiangsu Key Laboratory of Advanced Catalytic Materials and Technology, Changzhou University, 213164 Changzhou, China

Table of content

Characterization of catalysts.

The crystalline phases of the prepared materials were identified by X-ray diffraction (XRD) on a Rigaku powered diffraction unit with Cu Kα radiation (λ=1.5402 Å, 40 kV, 300 mA). Scanning electron micrograph (SEM) was performed on a ZEISS/SUPRA55 instrument. FTIR spectra of the prepared catalyst were collected on a Nicolet PROTÉGÉ 460 FTIR spectrometer using KBr disks. The inductively coupled plasma-atomic emission spectroscopy (ICP-AES) were carried out for quantitative analysis of metal elements using an Agilent ICPMS 7700. The N_2 adsorption–desorption isotherms were measured on a Micromeritics ASAP2460 at 77 K, and then the specific surface area was calculated by the Brunauer-Emmett-Teller (BET) method using the adsorption data in the relative pressure range from 0.05 to 0.30. The pore size distribution curves were calculated from analysis of the adsorption branch of the isotherm using the Barrett-Joyner-Halenda (BJH) method. Thermogravimetric analysis of samples are completed on ZRY-2P TG-DTG under the air atmosphere, the test temperature was 40~800 °C, and the heating rate was 10 °/min. X-ray photoelectron spectroscopy (XPS) patterns was achieved using a Thermo Scientific K-Alpha with a monochromatic Al X-ray source (excitation energy 1486.6 eV). The C 1s peak at 284.80 eV was used as calibration.

Typical procedure for Knoevenagel condensation between benzaldehyde and ethyl cyanoacetate.

Catalyst 10 mg, benzaldehyde (1 mmol), ethyl cyanoacetate (1 mmol) and DMF (3 mL) were added to a reaction tube, and the mixture was vigorously stirred at 35 °C under air. After the reaction, the reaction mixture was filtrated and 40 mg of nitrobenzene was added to the reaction solution. The products were analyzed using GC equipped with a FID detector and CP-Sil5 capillary column (length 50 m, i.d. 0.25 mm, film thickness 0.25 μm). Conversion and yield of products were determined based on benzaldehyde by GC using nitrobenzene as an internal standard. Products were also identified using standard compounds and GC-MS equipped with the same detector and capillary column.

SEM images (Fig. S1) indicate that the crystallinity of Ni_2Mg_2Mn-LDO increased and the flake structure disappeared after calcination.

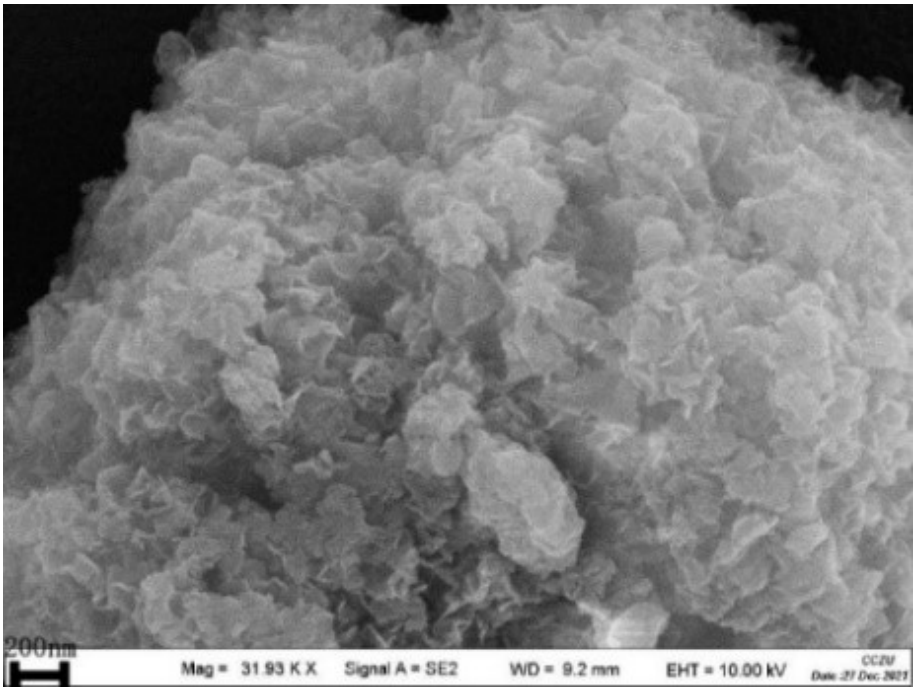

Fig. S1a. SEM image of Ni_2Mg_2Mn-LDH.

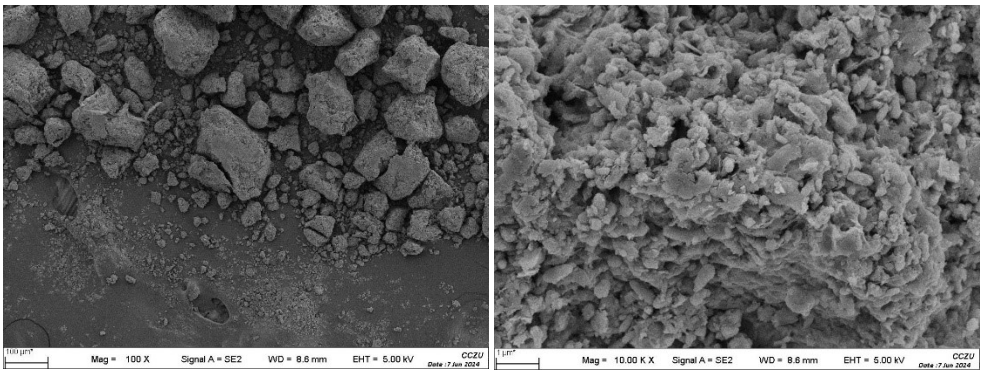

Fig. S1b. SEM images of Ni_2Mg_2Mn-LDO (250).

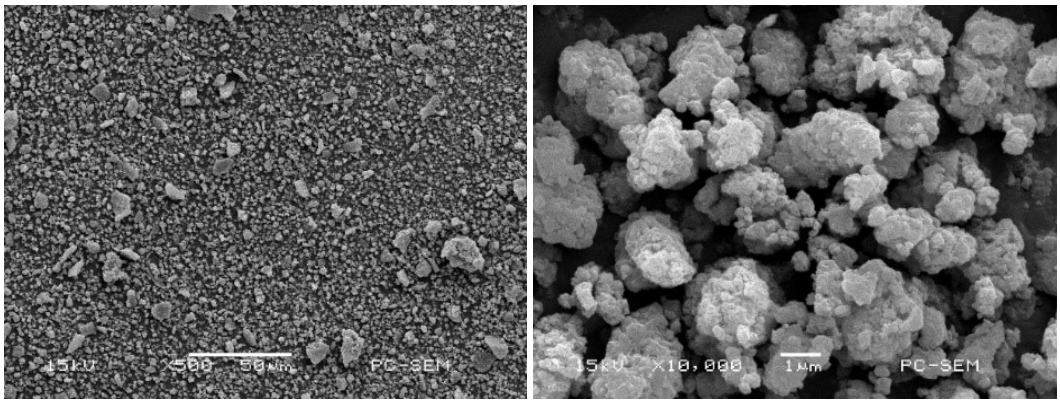

Fig. S1c. SEM images of Ni_2Mg_2Mn-LDO (350).

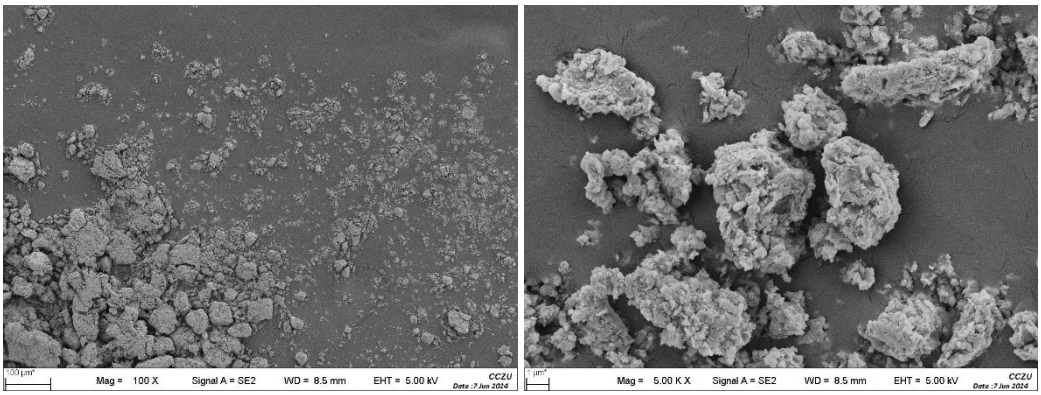

Fig. S1d. SEM images of Ni_2Mg_2Mn-LDO (450).

The thermogravimetric (TG) analysis of Ni_2Mg_2Mn-LDH and its calcined samples, depicted in Figure S2, outlines three distinct stages of weight loss. The initial weight loss around 100°C is attributed to the evaporation of surface-adsorbed water. Between 100°C and 200°C, the release of interlayer water occurs without the collapse of the hydrotalcite structure. The third stage, occurring between 200°C and 300°C, involves dehydration of hydroxyl groups on the brucite layers and the loss of CO_2 from the interlayers[1].

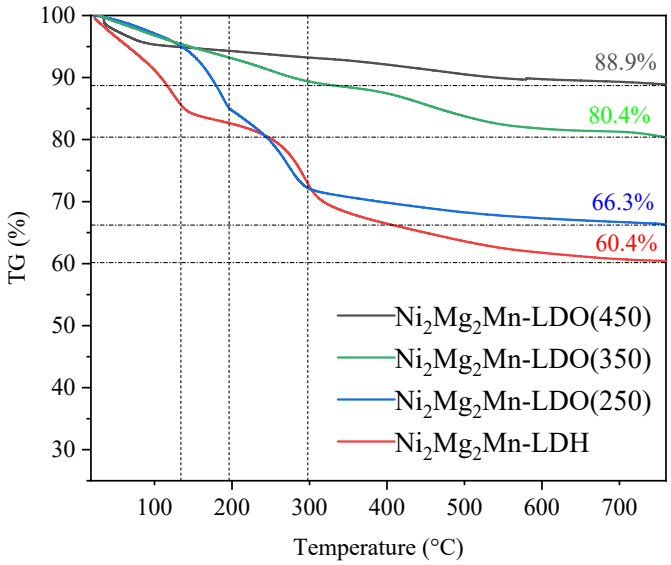

Fig. S2. TG thermogram of Ni_2Mg_2Mn-LDH, Ni_2Mg_2Mn-LDO (250), Ni_2Mg_2Mn-LDO (350) and Ni_2Mg_2Mn-LDO (450).

Fourier-transform infrared spectroscopy (FTIR) spectra of the four catalyst samples, displayed in Figure S3, confirm that mixed oxides gradually formed during calcination at various temperatures. The Ni_2Mg_2Mn-LDH spectra feature an absorption band near 3442 cm^{-1}, corresponding to the hydroxyl stretching vibrations of H_2O molecules. The peak at 1742 cm^{-1}, likely indicative of interlayer water, diminishes with the dehydration process during hydrotalcite calcination [2]. In the calcined samples, the

presence of hydroxyl groups or water, as indicated by spectral features, is due to the adsorption of atmospheric moisture during analysis. A distinct absorption peak at 1384 cm^{-1} in the Ni_2Mg_2Mn-LDH suggests the presence of carbonate anions; its absence in calcined samples indicates complete decarbonation post-calcination.

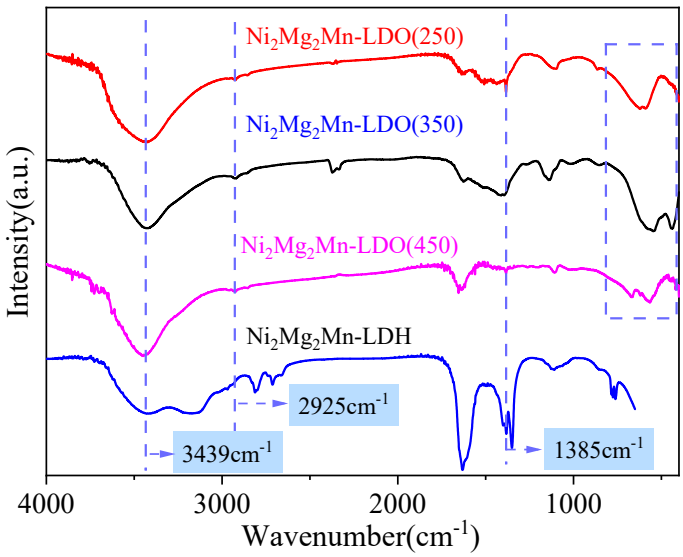

Fig. S3. FT-IR spectra of Ni_2Mg_2Mn-LDH and Ni_2Mg_2Mn-LDO (350).

Figure S4 displays the physical adsorption and desorption isotherms, as well as the pore size distributions, for the LDH samples, both before and after calcination. Both Ni_2Mg_2Mn-LDH and its thermally treated counterparts exhibit mesoporous characteristics. Their adsorption and desorption isotherms are classified as type IV isotherms, displaying hysteresis loops in the intermediate section. The hysteresis loop observed in the uncalcined Ni_2Mg_2Mn-LDH corresponds to the H3-type hysteresis loop, consistent with the characteristics of lamellar granular materials. This finding aligns with the analysis conducted using scanning electron microscopy. The specific surface area, pore volume, and pore size values are provided in Table S1. The calcined hydrotalcites all have a large specific surface area and pore volume, which may give Ni_2Mg_2Mn-LDO(350) a better catalytic performance for the decomposition of 1,2-diols. The specific catalytic effect depends on the quantity of active species and sites, necessitating confirmation through additional experiments.

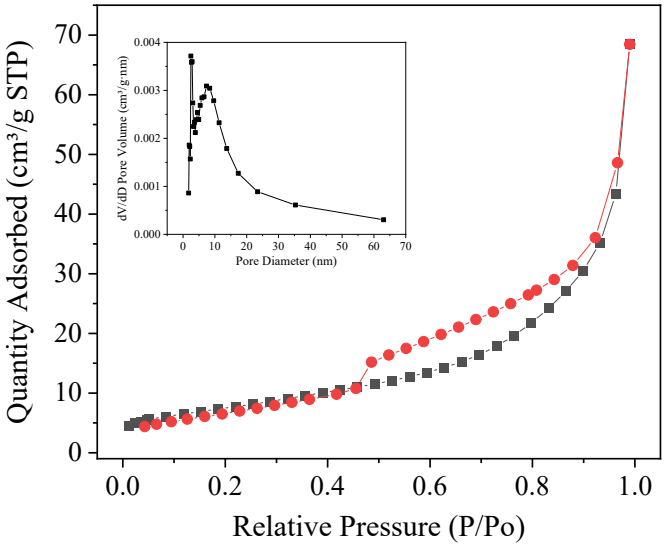

Fig. S4a. N_2 adsorption / desorption isotherms of Ni_2Mg_2Mn-LDH.

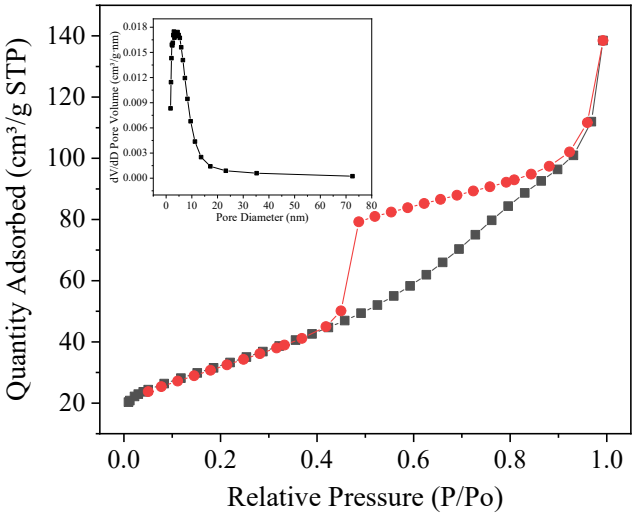

Fig. S4b. N_2 adsorption / desorption isotherms of Ni_2Mg_2Mn-LDO (250).

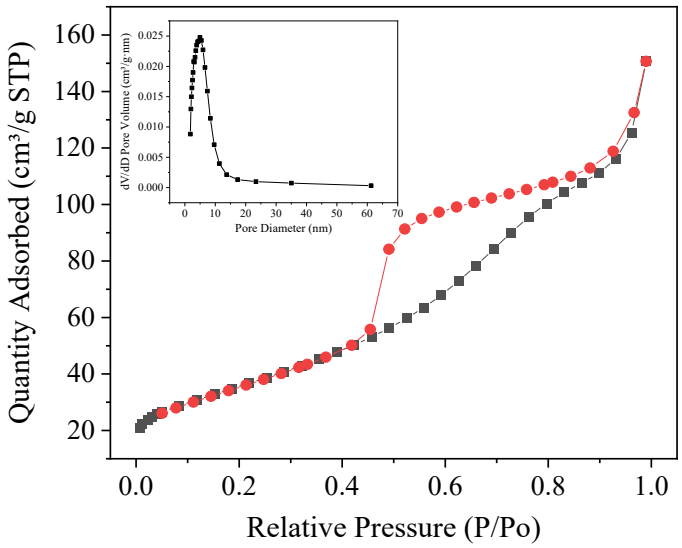

Fig. S4c. N_2 adsorption / desorption isotherms of Ni_2Mg_2Mn-LDO (350).

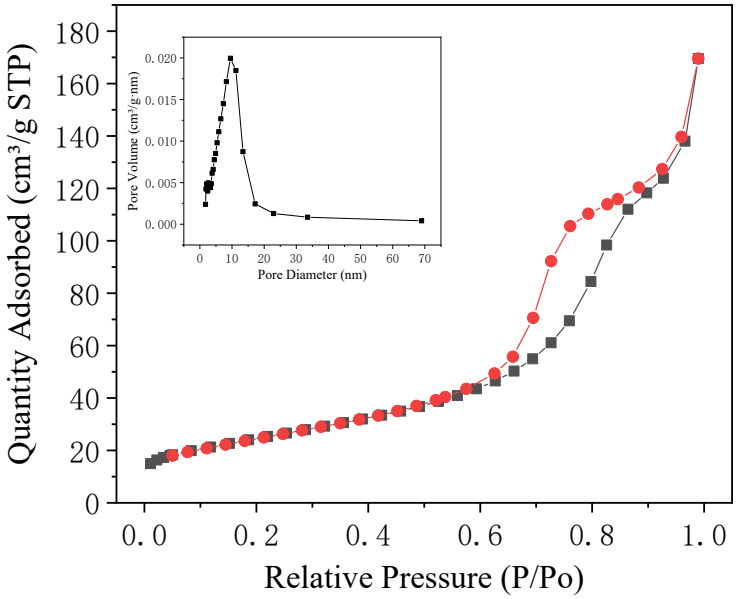

Fig. S4d. N_2 adsorption / desorption isotherms of Ni_2Mg_2Mn-LDO (450).

Table S1. Physico-chemical properties of Ni_2Mg_2Mn-LDH and Ni_2Mg_2Mn-LDO (350).

Entries	catalysts	surface area (m^2/g)	pore volume (cm^3/g)	Pore diameter (nm)
1	Ni_2Mg_2Mn-LDH	27.2869	0.105875	15.5203
2	Ni_2Mg_2Mn-LDO(250)	116.8115	0.214194	7.3347
2	Ni_2Mg_2Mn-LDO(350)	129.9681	0.233050	7.1725
4	Ni_2Mg_2Mn-LDO(450)	88.9210	0.262175	11.7936

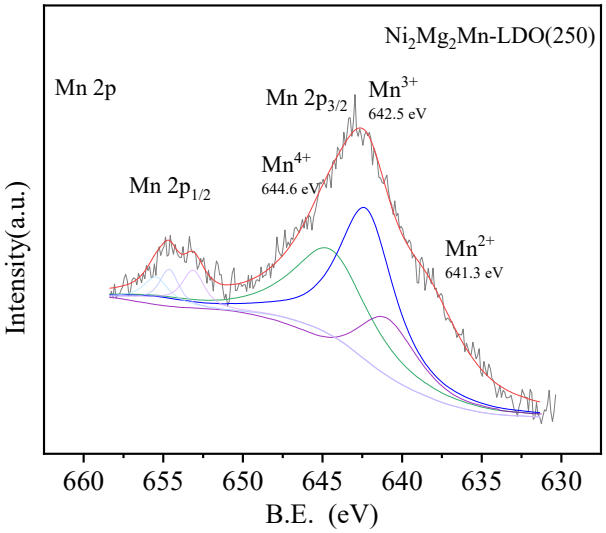

Fig. S5a. XPS diffraction patterns of Ni_2Mg_2Mn-LDO (250)

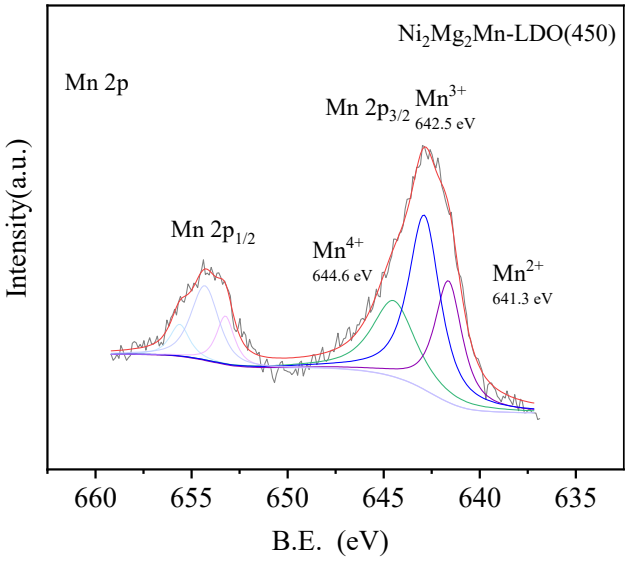

Fig. S5b. XPS diffraction patterns of Ni_2Mg_2Mn-LDO (450)

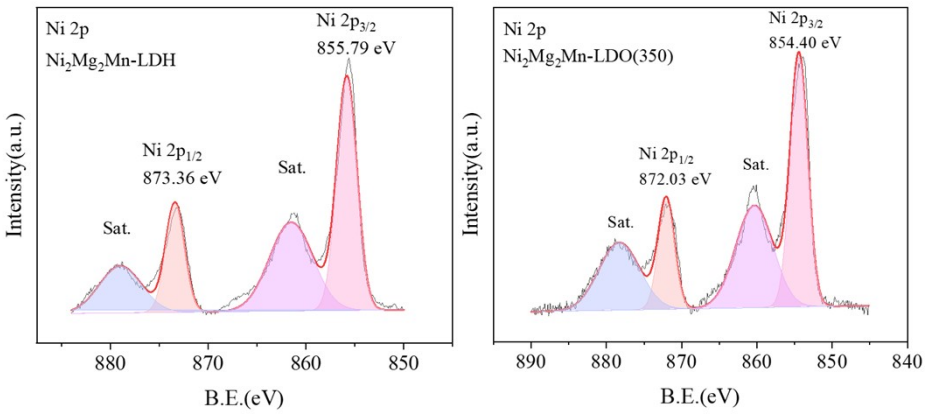

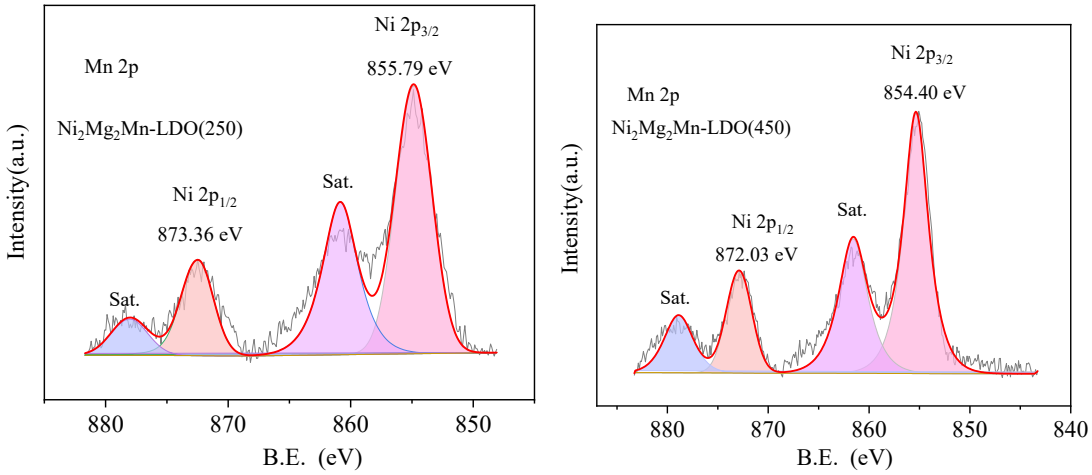

Fig. S5c. XPS diffraction patterns of prepared catalysts.

Table S2. Optimization of Reaction Conditions.

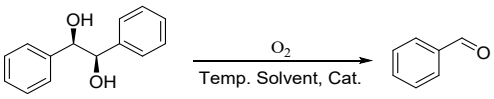

Entry		Catalyst	Conv. /%	Sel. /%
1	ethanol	Ni_2Mg_2Mn-LDO(250)	71	>99
2	ethanol	Ni_2Mg_2Mn-LDO(350)	99	>99
3	ethanol	Ni_2Mg_2Mn-LDO(450)	54	>99
4	ethanol	Ni_2Mg_2Mn-LDH	8	>99
5	H_2O	Ni_2Mg_2Mn-LDO(350)	trace	-
6	methanol	Ni_2Mg_2Mn-LDO(350)	28	>99
7	ethanol	-	trace	-
8[a]	ethanol	Ni_2Mg_2Mn-LDO(350)	6	>99
9[b]	ethanol	Ni_2Mg_2Mn-LDO(350)	55	>99
10	ethanol	activated MnO_2	36	>99
11	ethanol	Ni_2Mn-LDO(350)	16	>99
12	ethanol	Ni_2MgAl-LDO(350)	trace	-
13[c]	ethanol	Ni_2Mg_2Mn-LDO(350)	32	>99
14[d]	ethanol	Ni_2Mg_2Mn-LDO(350)	26	>99
15[e]	ethanol	Ni_2Mg_2Mn-LDO(350)	11	>99

Reaction conditions: *meso*-hydrobenzoin 0.25 mmol, catalyst 50 mg, ethanol 3 mL, 80 °C, 45 min, O_2 5 mL/min. [a] N_2. [b] air. [c] TEMPO. [d] BHT. [e] 1,4-Benzoquinone.

Reaction conditions were first investigated and presented in the supporting information in Table S2. Ethanol, a green solvent, was selected as the best solvent (Table S2, entry 2, 4, 5). A 99% conversion with complete selectivity toward benzaldehyde was obtained at 80 °C in ethanol within 45 min under O_2. Only Ni_2Mg_2Mn-LDO (350) showed satisfactory catalytic activity among the calcined samples and the

Ni_2Mg_2Mn-LDH precursor. Only 6% conversion can be obtained under N_2, confirming oxygen is essential for the reaction (Table S2, entry 8). The slight transformation under N_2 might be attributed to the absorbed oxygen on the surface of the catalyst materials. Mn and the alkalinity of the material are identified as pivotal factors influencing the reaction (Table S2, entry 10—12). The high catalytic activity of Ni_2Mg_2Mn-LDO (350) may be attributable to its high surface concentration of Mn^{3+} and basic sites, based on the result of the characters of the prepared materials.

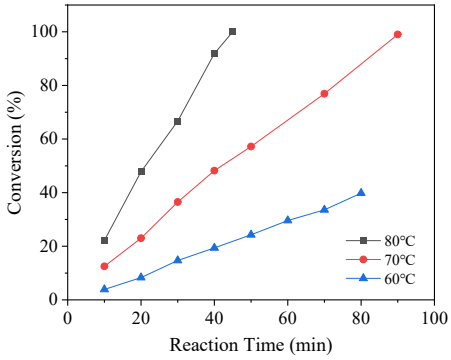

Fig. S6. Effect of reaction temperature and time.

The catalytic performance of the Ni_2Mg_2Mn-LDO(350) catalyst was investigated at 60°C, 70°C and 80°C, separately. It can be seen from the above figure that the conversion rate of hydrogen amine increases with the increase of temperature, and it can be roughly seen that the conversion rate increases exponentially with a 10°C rise in temperature. When the reaction temperature is 70°C, the reaction is complete within 90 min; and when the reaction temperature is 80°C, the reaction conversion can be completed within 45 minutes. Therefore, Ni_2Mg_2Mn-LDO(350) catalyzed the optimal reaction temperature for the oxidative decomposition of hydrogen amines at 80 °C and the optimal reaction time was 45 min.

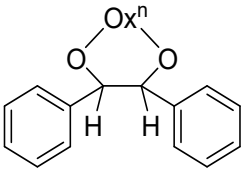

Scheme S1

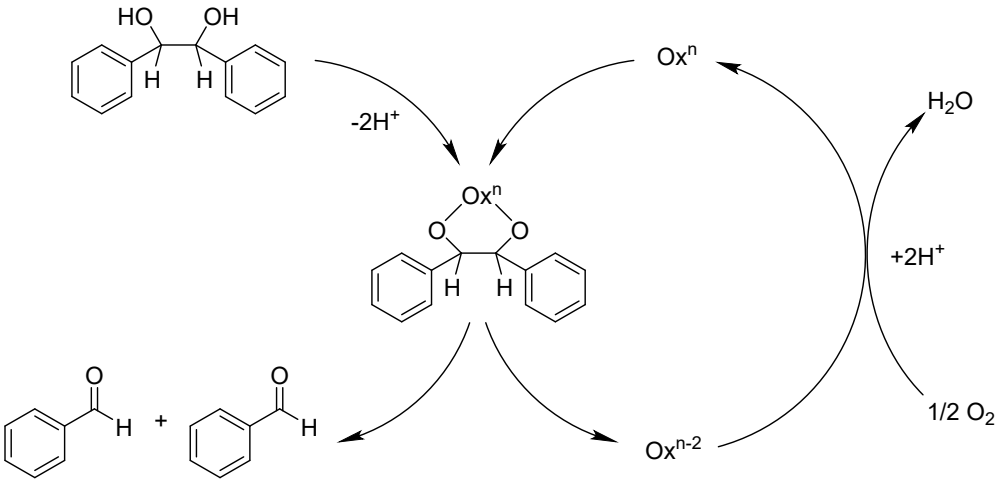

Scheme S2. Hypotheses regarding the mechanism involving cyclic intermediates.

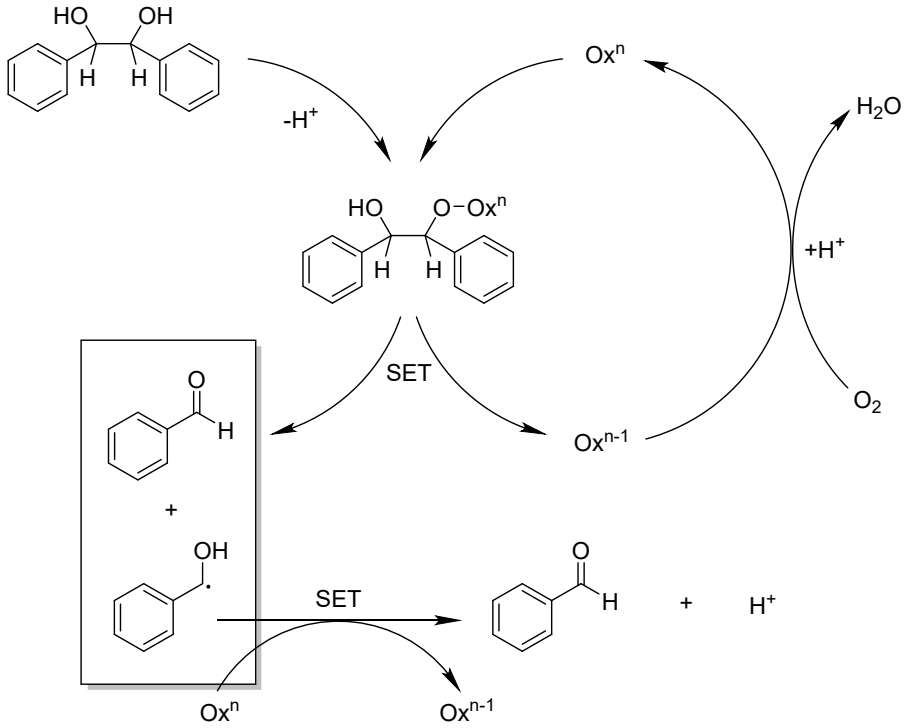

Scheme S3. Hypothesis regarding the mechanism of single-electron transfer.

Kinetic experiments

Out-diffusion exclusion

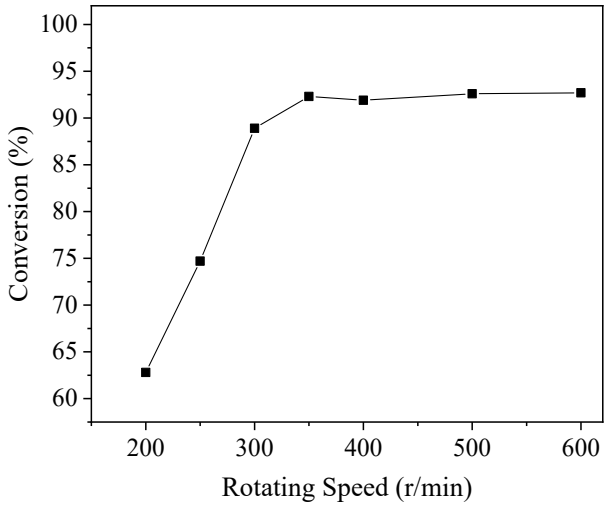

Fig. S7. The effect of rotational speed on the conversion of the oxidative decomposition of hydrogen amines.

The external diffusion effect was investigated by adjusting the rotational speed. And the results depicted in Fig. S6 show that external diffusion could be neglected when the rotational speed was higher than 350 /min in the oxidative decomposition of hydrogen amines. The influence of internal diffusion was eliminated through calculation.

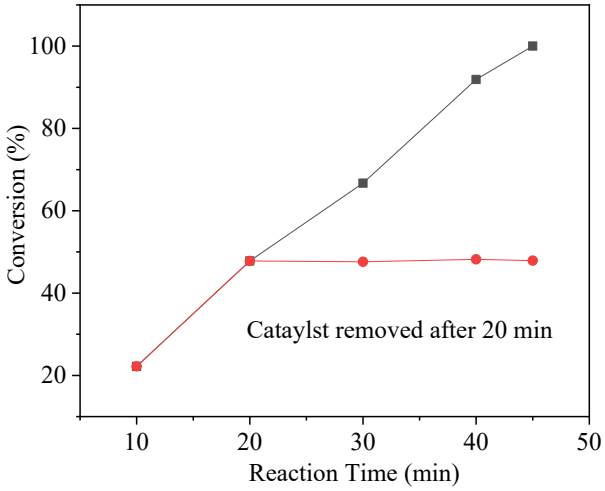

Fig. S8. The hot-filtration experiment.

Reaction conditions: (*R,R*)-hydrobenzoin 0.25 mmol, ethanol 3 mL, Ni_2Mg_2Mn-LDO(350) 50 mg, 80 ℃, O_2 5 mL/min.

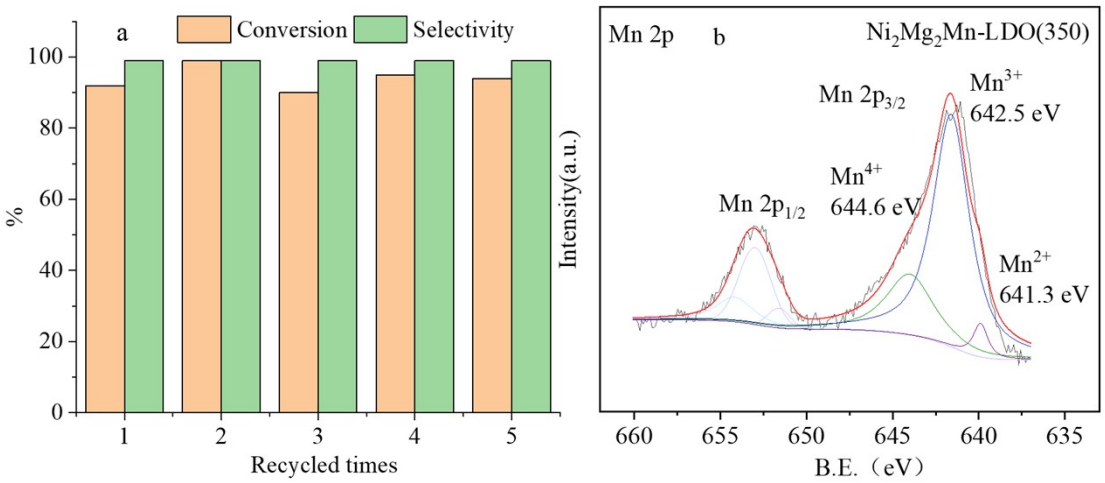

Fig. S9a. The recycled results of Ni_2Mg_2Mn-LDO(350) catalyst.

Reaction conditions: (*R,R*)-hydrobenzoin 0.25 mmol, ethanol 3 mL, Ni_2Mg_2Mn-LDO(350) 50 mg, 80 ℃, O_2 5 mL/min.

Fig. S9b. XPS diffraction patterns of recycled Ni_2Mg_2Mn-LDO(350)

Analytical Data

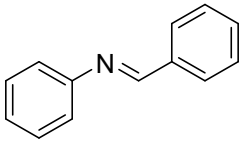

(E)-N,1-diphenylmethanimine

Pale yellow solid; ^{1}H NMR (400 MHz, Chloroform-*d*) δ 8.44 (s, 1H), 7.94 – 7.84 (m, 2H), 7.46 (dd, *J* = 5.1, 1.9 Hz, 3H), 7.41 – 7.30 (m, 2H), 7.22 (tt, *J* = 8.3, 1.2 Hz, 3H). ^{13}C NMR (101 MHz, Chloroform-d) δ 160.4, 152.0, 136.1, 131.3, 129.1, 128.8, 128.7, 125.9, 120.8. HRMS (ESI) Calcd. for $C_{11}H_{12}O_2$ $[M+H]^+$ 182.0964, found 182.0959.

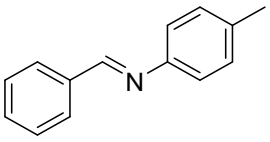

Phenyl-N-(p-tolyl)methanimine

Yellow oil; ^{1}H NMR (300 MHz, Chloroform-*d*) δ 8.34 (s, 1H), 7.83 – 7.74 (m, 2H), 7.39 – 7.28 (m, 3H), 7.13 – 6.98 (m, 4H), 2.25 (s, 3H). ^{13}C NMR (75 MHz, Chloroform-*d*) δ 159.5, 149.3, 136.2, 135.7, 131.1, 129.7, 128.6, 128.6, 120.7, 20.9. HRMS (ESI) Calcd for $C_{11}H_{12}O_2$ $[M+H]^+$ 196.1121, found 196.1118.

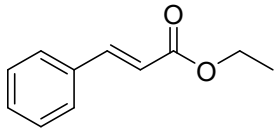

Ethyl cinnamate

^{1}H NMR (400 MHz, Chloroform-*d*) δ 7.69 (d, *J* = 16.0 Hz, 1H), 7.55 – 7.50 (m, 2H), 7.41 – 7.33 (m, 3H), 6.45 (d, *J* = 16.0 Hz, 1H), 4.17 (t, *J* = 6.7 Hz, 2H), 1.78 – 1.69 (m, 2H), 0.99 (t, *J* = 7.4 Hz, 3H). ^{13}C NMR (101 MHz, Chloroform-*d*) δ 167.1, 144.5, 134.4, 130.2, 128.8, 128.0, 118.2, 66.1, 22.0, 10.4. HRMS (ESI) Calcd. for C11H12O2 $[M+H]^+$ 177.0910, found 177.0909.

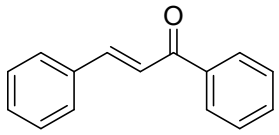

(E)-chalcone

Light Yellow solid; ^{1}H NMR (400 MHz, Chloroform-*d*) δ 8.08 – 7.97 (m, 2H), 7.81 (d, *J* = 15.7 Hz, 1H), 7.65 – 7.62 (m, 2H), 7.61 – 7.46 (m, 4H), 7.45 – 7.37 (m, 3H). ^{13}C NMR (101 MHz, Chloroform-d) δ 190.5, 144.8, 138.1, 134.8, 132.7, 130.5, 128.9, 128.6, 128.4, 128.4, 122.0. HRMS (ESI) Calcd. for C11H12O2 $[M+H]^+$ 209.0961, found 209.0956.

NMR Spectra

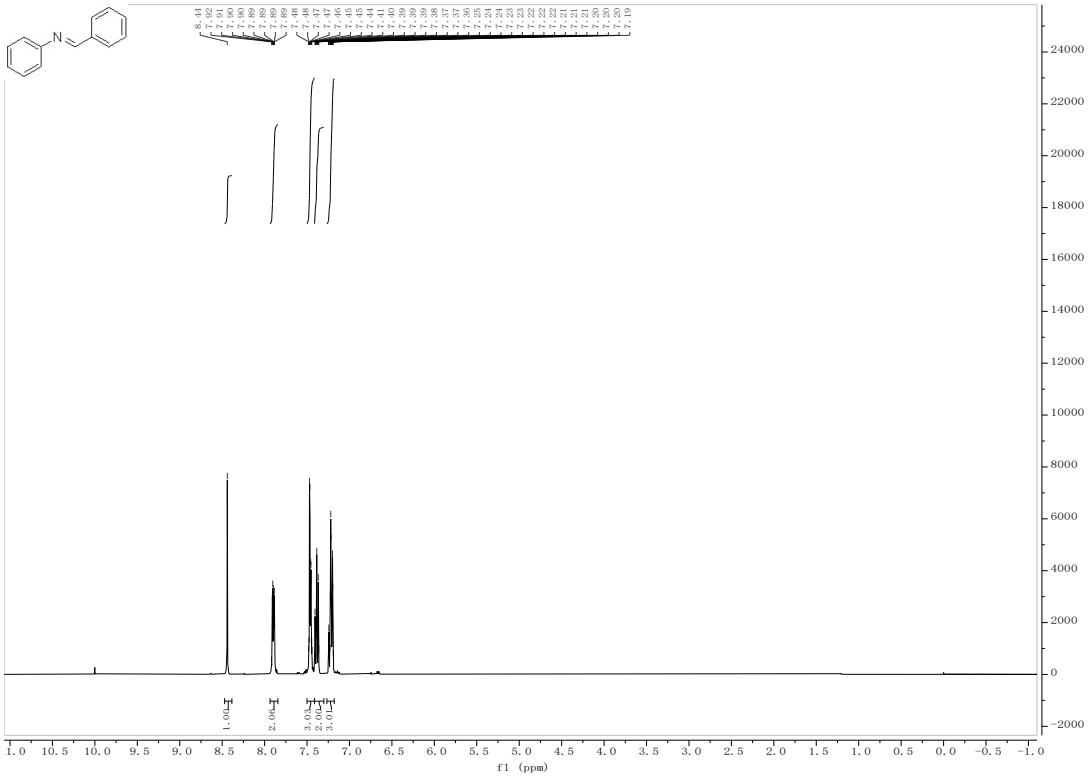

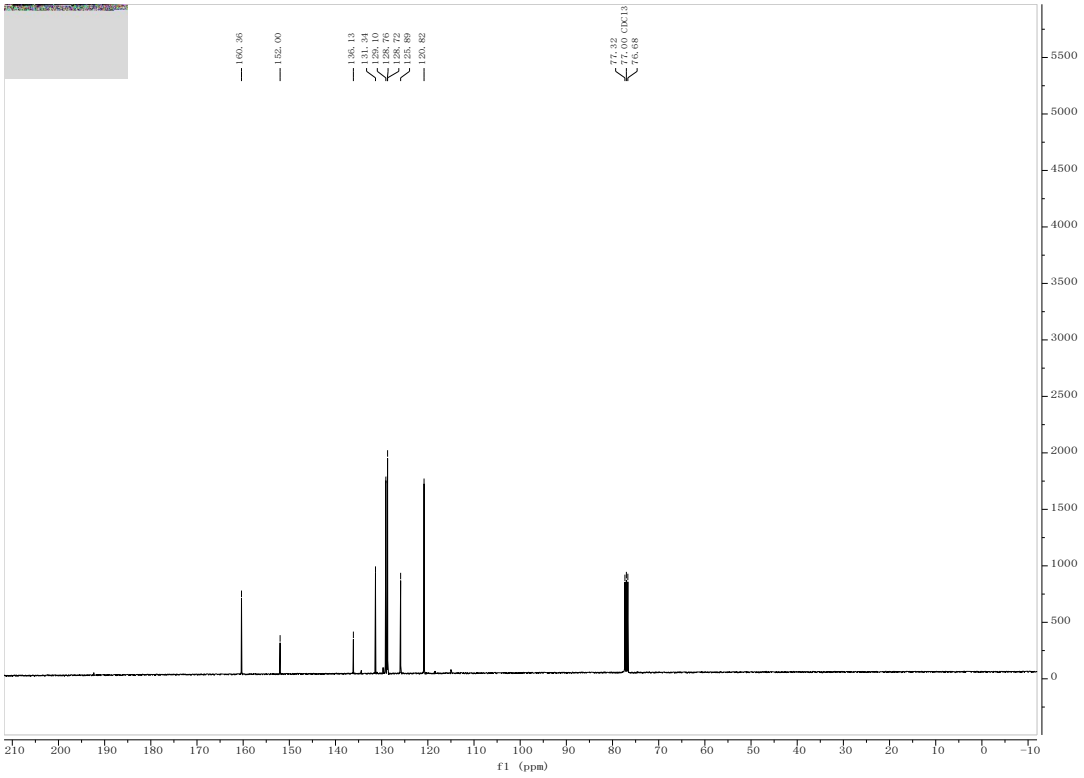
160.36
152.00
136.13
131.34
129.10
128.76
128.72
125.89
120.82
77.32
77.00 CDCl3
76.68
f1 (ppm)

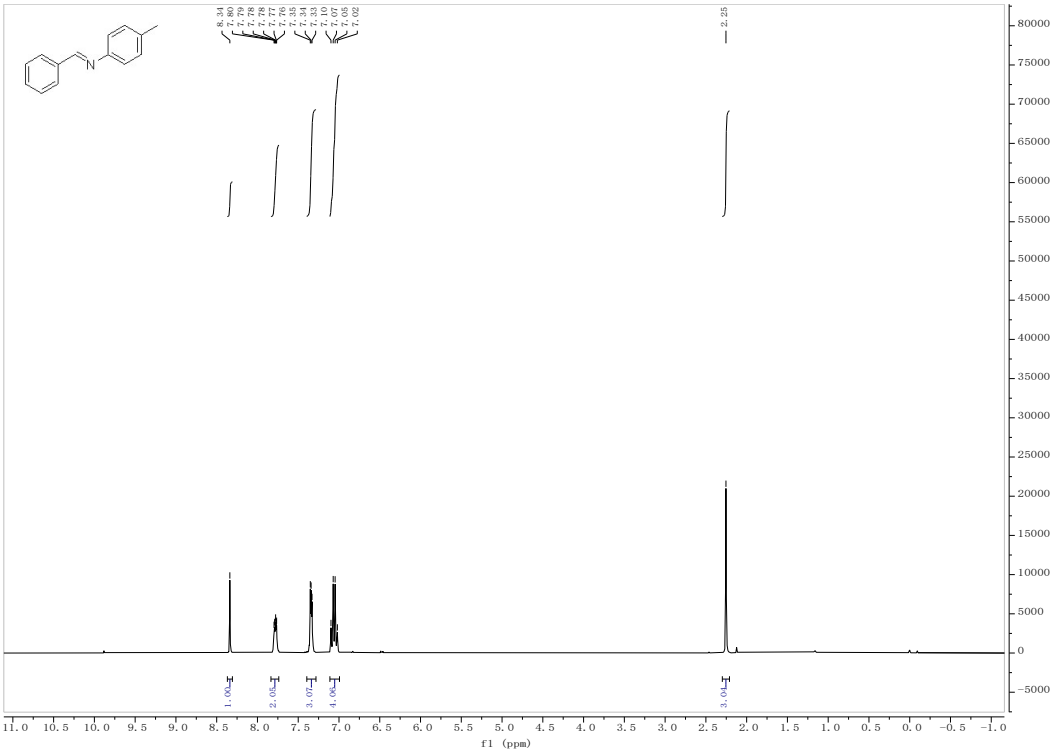
8.34
7.80
7.79
7.78
7.78
7.77
7.76
7.35
7.34
7.33
7.10
7.07
7.05
7.02
2.25
1.00
2.05
3.07
4.06
3.04
f1 (ppm)

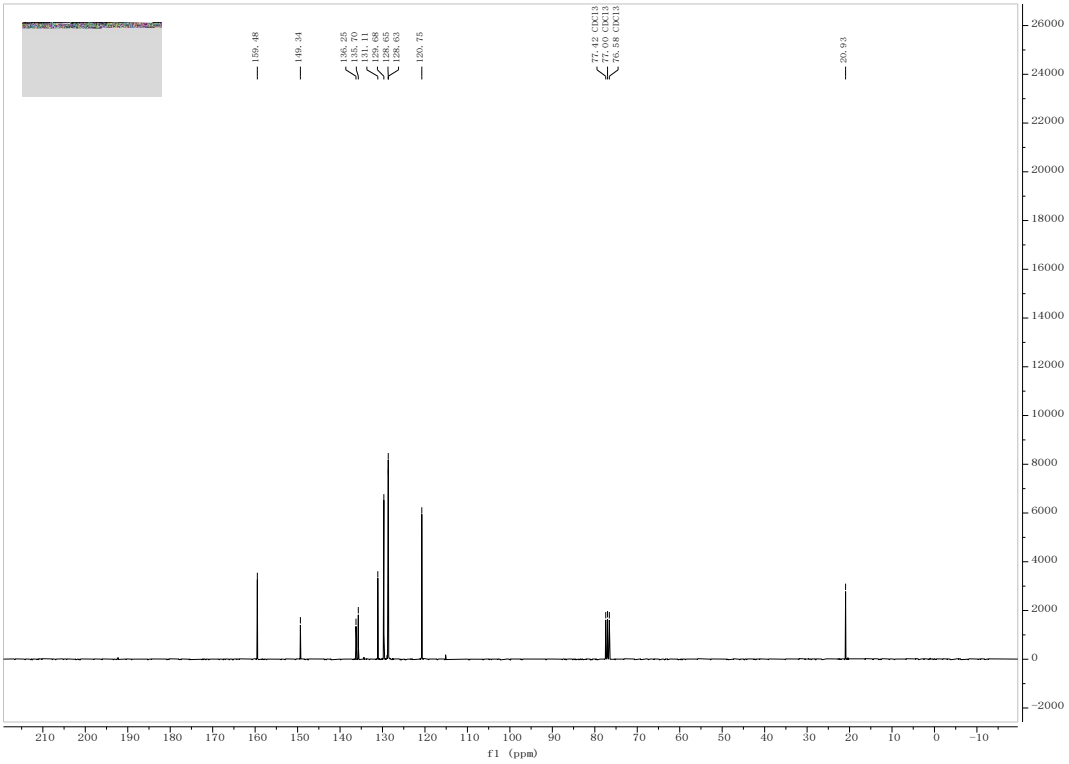
159.48
149.34
136.25
135.70
131.11
129.68
128.65
126.63
120.75
77.42 CDCl3
77.00 CDCl3
76.58 CDCl3
20.93
f1 (ppm)

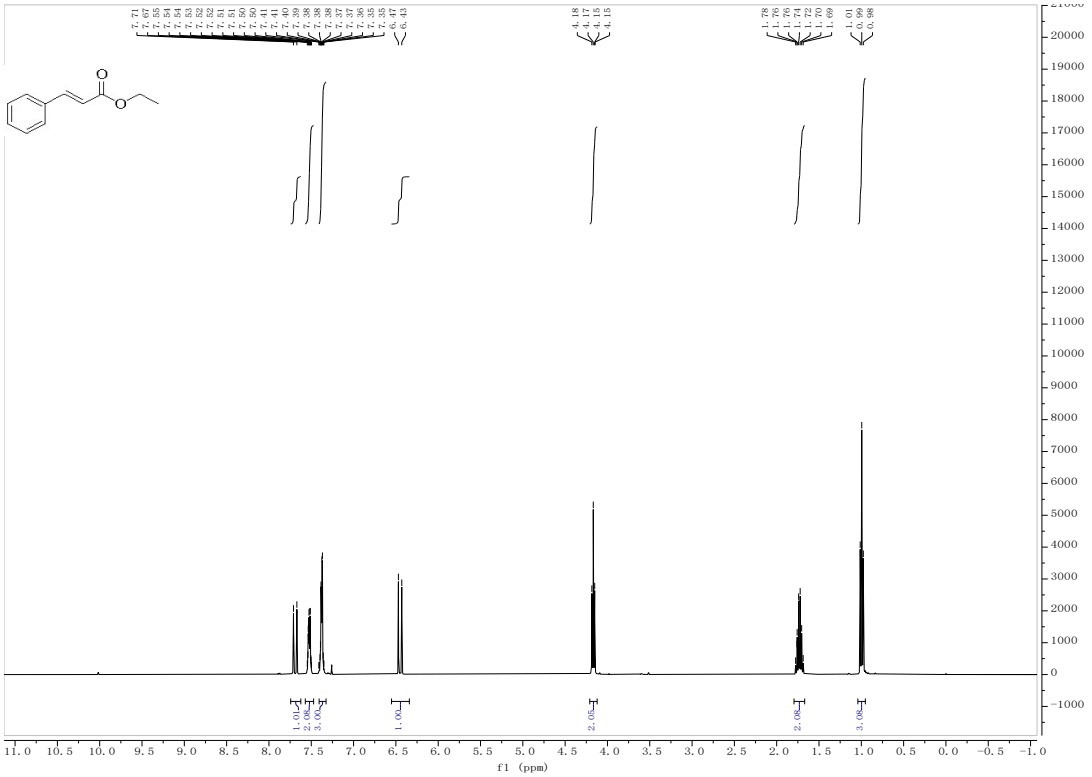
7.71
7.67
7.55
7.54
7.54
7.53
7.52
7.52
7.51
7.51
7.50
7.50
7.41
7.41
7.40
7.39
7.38
7.38
7.37
7.37
7.36
7.35
7.35
6.47
6.43
4.18
4.17
4.15
4.15
1.78
1.76
1.76
1.74
1.74
1.72
1.70
1.69
1.01
0.99
0.98
1.01
2.08
3.00
1.00
2.05
2.08
3.08
f1 (ppm)

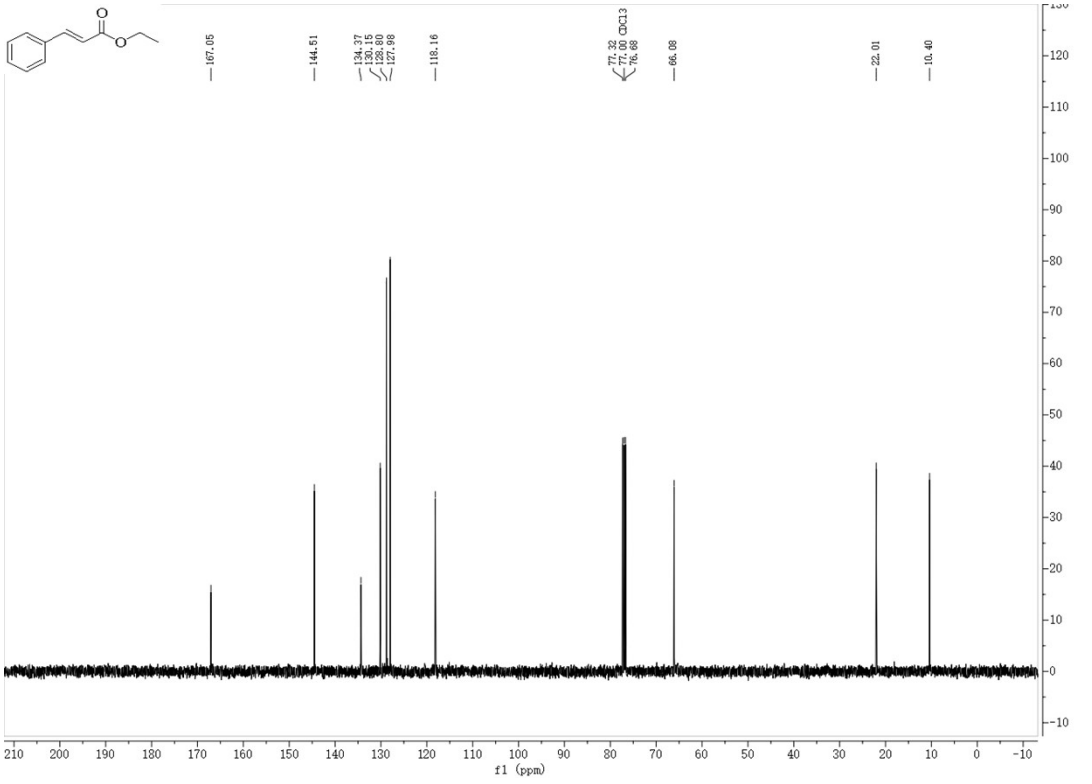
167.05
144.51
134.37
130.16
128.60
127.98
118.16
77.32
77.00
CDCl3
76.68
66.08
22.01
10.40
f1 (ppm)

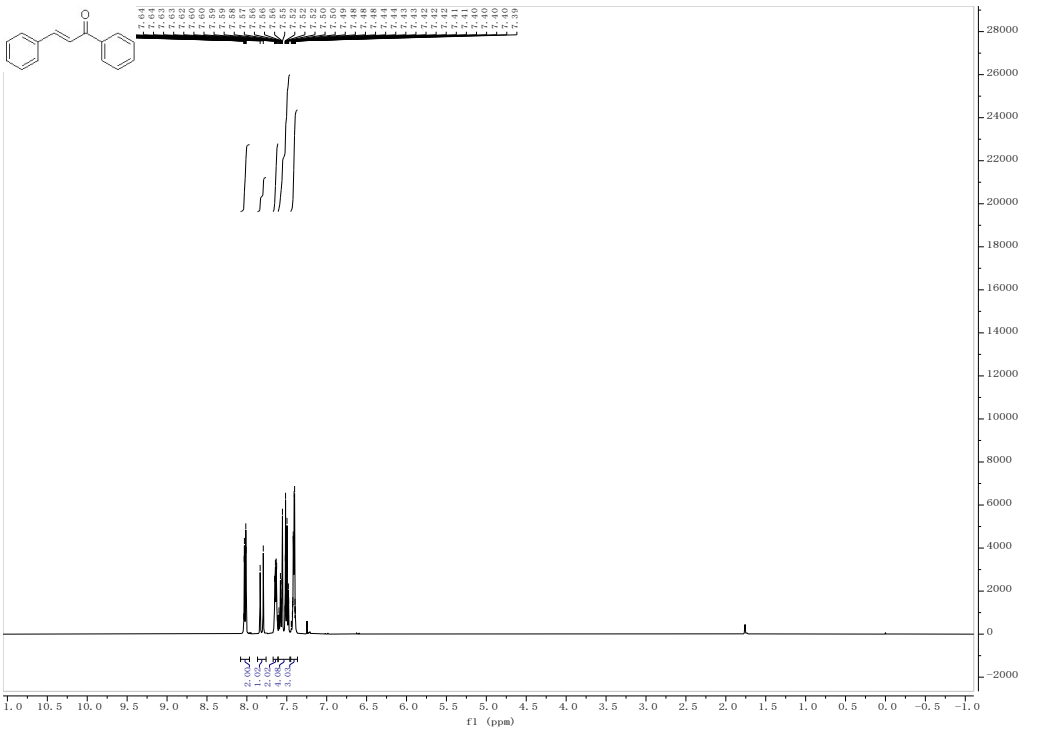
7.64
7.64
7.63
7.63
7.62
7.60
7.60
7.59
7.59
7.58
7.57
7.56
7.56
7.55
7.52
7.52
7.50
7.49
7.48
7.48
7.44
7.43
7.43
7.42
7.42
7.41
7.41
7.40
7.40
7.39
2.00
1.02
2.01
4.06
3.02
f1 (ppm)

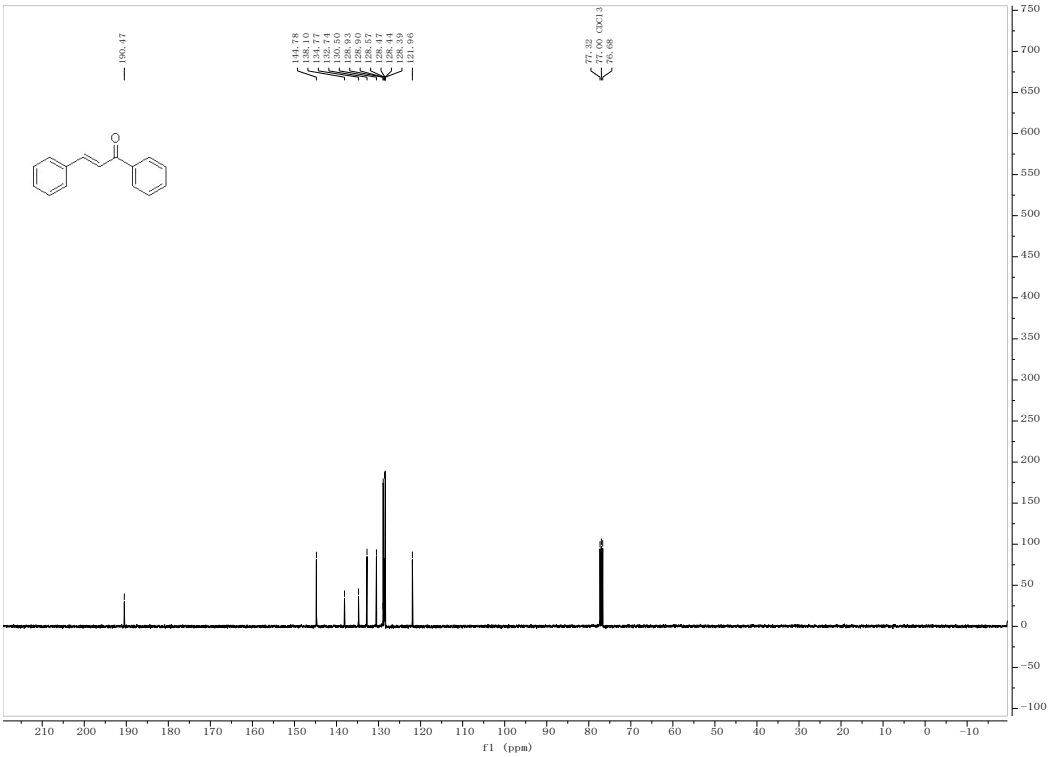
190.47
144.78
138.10
134.77
132.74
130.50
128.93
128.90
128.57
128.47
128.44
128.39
121.96
77.22
77.00
CDCl3
76.68
f1 (ppm)

Reference

[1] J. Pérez-Ramírez, G. Mul, F. Kapteijn, J.A. Moulijn, In situ investigation of the thermal decomposition of Co–Al hydrotalcite in different atmospheres, J. Mater. Chem., 11 (2001) 821-830.

[2] Pérez-Ramírez J, Mul G, Kapteijn F, *et al*. Insitu investigation of thethermal decomposition of Co-Al hydrotalcite in different atmospheres [J]. *Journal of Materials Chemistry*, **2001**, 11(3): 821-830.